PERGAMON

International Journal of Heat and Mass Transfer 45 (2002) 815–829

International Journal of HEAT and MASS TRANSFER

www.elsevier.com/locate/ijhmt

Prediction of turbine blade heat transfer and aerodynamics using a new unsteady boundary layer transition model

M.T. Schobeiri *, P. Chakka

Department of Mechanical Engineering, Turbomachinery Performance and Flow Research Laboratory, Texas A & M University, College Station, TX 77843-3123, USA

Received 18 August 2000; received in revised form 21 May 2001

Abstract

The effects of periodic unsteady flow on heat transfer and aerodynamic characteristics, particularly on the boundary layer transition along the suction and the pressure surfaces of a typical gas turbine blade, are experimentally and theoretically investigated. Comprehensive aerodynamic and heat transfer experimental data are collected for different unsteady passing frequencies that are typical of gas turbines. To predict the effect of the impinging periodic unsteady flow on the heat transfer and the aerodynamics of turbine blades, a new unsteady boundary layer transition model is developed. The model is based on a universal unsteady intermittency function and utilizes an inductive approach that implements the results of comprehensive experimental and theoretical studies of unsteady wake development and the boundary layer flow. Three distinct quantities are identified as primarily responsible for the transition of an unsteady boundary layer: (1) the universal relative intermittency function, (2) maximum intermittency, and (3) minimum intermittency. The analysis of the experimental results and the comparison with the model prediction confirm the validity of the model and its capability to accurately predict the unsteady boundary layer transition. © 2001 Published by Elsevier Science Ltd.

Keywords: Unsteady; Boundary layer transition; Turbine blades

1. Introduction

The flow in a turbomachine stage is highly turbulent and unsteady due to the interactions between the stator and the rotor. The trailing edge thickness, together with the boundary layer thickness, in association with the rotational motion of the rotor generates unsteady wakes. The unsteady wake exhibits mean velocity defects with a high level of turbulence intensity that passes through the blade rows affecting the natural boundary layer transition. The effect of these wakes on boundary layer transition is important to the design of turbomachinery blades. Successful prediction of transition start and length would help in designing efficient turbine or compressor stages. However, the transition process under the influence of periodic unsteady wakes is not predicted reliably with the existing steady transition models. For this reason, the current investigation focuses on the transition process and its effect on the boundary layer velocity profiles and heat transfer coefficients under unsteady wake flow condition.

The transition process was first explained by Emmons [1] through the turbulent spot production theory. This theory was later promoted by Dhawan and Narasimha [2], who proposed a universal profile for intermittency factor for natural transition. Studies by Abu-Ghannam and Shaw [3], Gostelow and Blunden [4], Dullenkopf and Mayle [5], Gostelow et al. [6] were conducted to determine the effect of free-stream turbulence and pressure gradient on the spot production rate and the intermittency factor. Experiments for the effect of unsteady wake flow on the boundary layer transition

* Corresponding author. Tel.: +1-979-845-0819; fax: +1-979-845-3081.

E-mail address: tschobeiri@mengr.tamu.edu (M.T. Schobeiri).

0017-9310/02/$ - see front matter © 2001 Published by Elsevier Science Ltd.
PII: S0017-9310(01)00190-9

Nomenclature

b	intermittency wake width
c	blade chord
C	threshold level
C_p	pressure coefficient, $C_p = (p - p_{ref})/\frac{1}{2}\rho U_{in}^2$
h	heat transfer coefficient
$I(t)$	step function (square wave)
Nu	Nusselt number based on concave arc length, $Nu = hs_0/k$
Pr	Prandtl number, $Pr = v/\alpha$
p_{ref}	test section inlet static pressure
Re_c	Reynolds number based on blade chord, $U_{in}c/v$
Re_x	local Reynolds number based on longitudinal distance, $Re_x = (\overline{U}s)/v$
$Re_{x,s}$	Reynolds number at the beginning of transition
$Re_{x,e}$	Reynolds number at the end of transition
s	longitudinal distance from plate leading edge (mm)
s_0	streamwise distance from the leading edge of the blade
s_R	rod spacing
S_B	blade spacing, 160 mm
$S(t)$	detector function
St	Stanton number, $St = h/(\rho C_p \overline{U})$
t	time (s)
T	time for one revolution of wake generator
T_{yl}	yellow line temperature of the liquid crystals, 45°C
T_∞	air temperature at the inlet of test section
Tu	reference turbulence intensity
$\langle Tu \rangle$	ensemble-averaged reference turbulence intensity
U	instantaneous velocity (m/s)
$\overline{U}$	time-averaged velocity (m/s)
U_{in}	inlet velocity in streamwise direction (m/s)
U_w	circumferential velocity of the wake generator, belt translational velocity (m/s)
y	lateral distance from plate surface (mm)

Greek symbols

α	thermal diffusivity (m^2/s)
$\langle \gamma(t) \rangle_{max}$	maximum ensemble-averaged intermittency
$\langle \gamma(t) \rangle_{min}$	minimum ensemble-averaged intermittency
$\overline{\gamma}$	time-averaged intermittency
$\langle \gamma(t) \rangle$	ensemble-averaged intermittency
Γ	relative turbulence intermittency
ϵ	eddy diffusivity, emissivity
ζ	non-dimensional coordinate, ξ_2/b
v	kinematic viscosity of air (m^2/s)
ξ_2	transformed coordinate, $\xi_2 = ts_R/\tau$
ρ	density of air (kg/m^3)
σ	blade chord spacing ratio c/S_B, Stefan–Boltzmann constant (heat transfer)
τ	one wake passing period
ϕ	velocity ratio, U_{in}/U_w
Ω	non-dimensionalized unsteady parameter, $\Omega = (\sigma S_B)/(\phi S_R)$

Superscripts and subscripts

-	time-averaged
eff	effective
H, M	heat, momentum

were conducted by Walker [7], Hodson [8], Paxson and Mayle [9] and Orth [10]. Hodson developed a method for calculating boundary layer parameters under unsteady flow conditions using the strip calculation method and space–time diagrams. He compared the loss coefficient for a turbine blade calculated using the strip calculation method with time-averaged results. Paxson and Mayle [9] investigated the effect of unsteady passing wakes on the laminar boundary layer near the stagnation region. Dullenkopf and Mayle [5] proposed a time-averaged transition model. Although this model produces satisfactory results, it is not appropriate for the unsteady flow situation. Few of these researchers have addressed the effect of wake frequency and the structure on boundary layer transition.

Calculating the intermittency factor under the unsteady flow situation is a difficult task because of the free-stream, which periodically changes from almost non-turbulent to high turbulent intensity values. The process of turbulent/non-turbulent decisions from the instantaneous signals measured under these unsteady conditions is reviewed by Hedley and Keffer [11]. They proposed derivatives of velocity signals as the detector function to identify the turbulent and non-turbulent parts in the signals. This method was also used by Kovasznay et al. [12], Antonia and Bradshaw [13], and Bradshaw and Murlis [14]. Paxson and Mayle [9] and Mayle [15] used a similar method for unsteady flows.

Developing an accurate unsteady transition model is essential to predict the unsteady boundary layer characteristics such as skin friction and heat transfer coefficients. With an appropriate transition model, it is possible to solve the boundary layer equations numerically using the methods proposed by Launder and Spalding [16], Crawford and Kays [17], and Schmidt and Patankar [18]. Bearing this in mind, the current investigation focuses on calculating the intermittency factor and developing an unsteady model that can be used in Navier–Stokes and boundary layer codes to predict the

parameters necessary for the efficient design of turbomachinery stages.

The present investigation includes aerodynamic and heat transfer experiments detailed in Section 2 to provide a comprehensive set of data. Instantaneous velocity signals are used to determine the intermittency throughout the boundary layer. Details on the calculation and analysis of intermittency for unsteady flows are discussed in Section 3. The implementation of the model in the boundary layer code is explained in Section 4, followed by the results and discussion.

2. Experimental investigations

To understand the effect of unsteady wakes on the aerodynamic and heat transfer characteristics, detailed experiments are performed on the suction and pressure surfaces of a turbine blade. The experimental data are collected using a high-subsonic wind tunnel test facility, shown in Fig. 1. Since this facility was already described by Schobeiri et al. [19] only a brief description will be given below.

The facility consists of a large centrifugal fan, a settling chamber, a nozzle, a wake generator, and a cascade test section. Through the use of a throttle mechanism located at the exit of the fan, the velocity at the inlet of the test section is set at 15 m/s. The rest of the inlet flow conditions can be found in Table 1. The free-stream turbulence intensity of steady flow into the test section is 1.0%. As explained by Schobeiri et al. [19], the facility was designed to generate a turbulence intensity of about 0.75% without wakes. For unsteady flow cases, however, higher free-stream turbulence intensities are established by wakes.

The cascade test section, shown in Fig. 1(b), is located downstream of the wake generator. Using a nozzle with a height of 1000 mm and a width of 200 mm, the test section can include up to seven blades with a height of 200 mm and the chord up to 250 mm. The blades are inserted between two vertical plexiglass side walls. One sidewall integrated the boundary layer, the inlet, and the exit traversing slots. The turbine blades used for experimentation are specially manufactured for specific measurements. For boundary layer measurements, five NASA turbine blades are implemented whose geometry is described in the NASA Report by Schobeiri et al. [20]. One of these aerodynamic blades is specially manufactured for static pressure measurements over the blade surface. A separate blade is manufactured with a copper internal core for heat transfer measurements. A sheet of liquid crystal is glued onto the surface of the heat transfer blade for temperature measurements.

Two-dimensional periodic unsteady flow is simulated by the translational motion of a wake generator (see Fig. 1), with a series of cylindrical rods attached to two parallel operating timing belts driven by an electric motor. The distance between the wake generator rods and the leading edge of the turbine blade is 108 mm. The research facility allows measurements of up to four frequency ranges in one revolution. This is done by attaching up to four clusters of rods with different spacings to the two parallel timing belts with a circumference of 5000 mm moving with translational motion. One of the four clusters has no rods, thus simulating the steady case. The data acquisition and analysis system separates and regroups the data before applying the unsteady ensemble average technique. The special design of the facility and the length of the belts enable considerable reduction of the measurement time when performing the boundary layer experiments. The unsteady flow produced by the wake generator is characterized by an unsteady parameter Ω. This parameter, similar to the Strouhal number, is defined as $\Omega = (\sigma/\phi)(S_B/s_R)$, where σ is the cascade solidity and ϕ is the flow coefficient. The values of Ω cover a broad range that are typical of a turbomachine and are specified in Table 1.

2.1. Boundary layer velocity measurements

A single hot-wire probe is used to measure instantaneous velocities inside the boundary layer. The probes are calibrated in a separate facility exclusively designed for this purpose, and the details of the calibration can be found in John and Schobeiri [21]. Measurements are taken at 14 and 10 axial locations on the suction and pressure surfaces, respectively. A computer controlled traversing system with encoder moves the probe in the lateral direction (perpendicular to the blade surface) for measurements inside the boundary layer and close to the wall. The traversing system is designed to increment in steps of 2.5 μm, which is necessary for critical boundary layer data. The measurements are taken at 39 locations in the lateral direction giving a comprehensive set of data for critical analysis of the transition process. For the present investigation, two clusters of rods with constant diameter are attached to the belts. The cylindrical rods within each cluster have the same spacing. This setup makes it possible to sequentially measure the effect of two different spacings at a single boundary layer point. To clearly define the influence domain of each individual cluster with the other one, the clusters are arranged with a certain distance between each other. Three wake frequencies that correspond to Ω values of 0, 0.755 and 1.51 are used to collect of aerodynamic data. At each position, 16,384 samples were taken at a sampling rate of 20 kHz for each of 50 revolutions of the wake generator. The data were ensemble-averaged with respect to the rotational period of the wake generator. Before final data were taken, the number of samples per revolution and the total number of revolutions were varied to determine the optimum settings for the convergence of the ensemble-average.

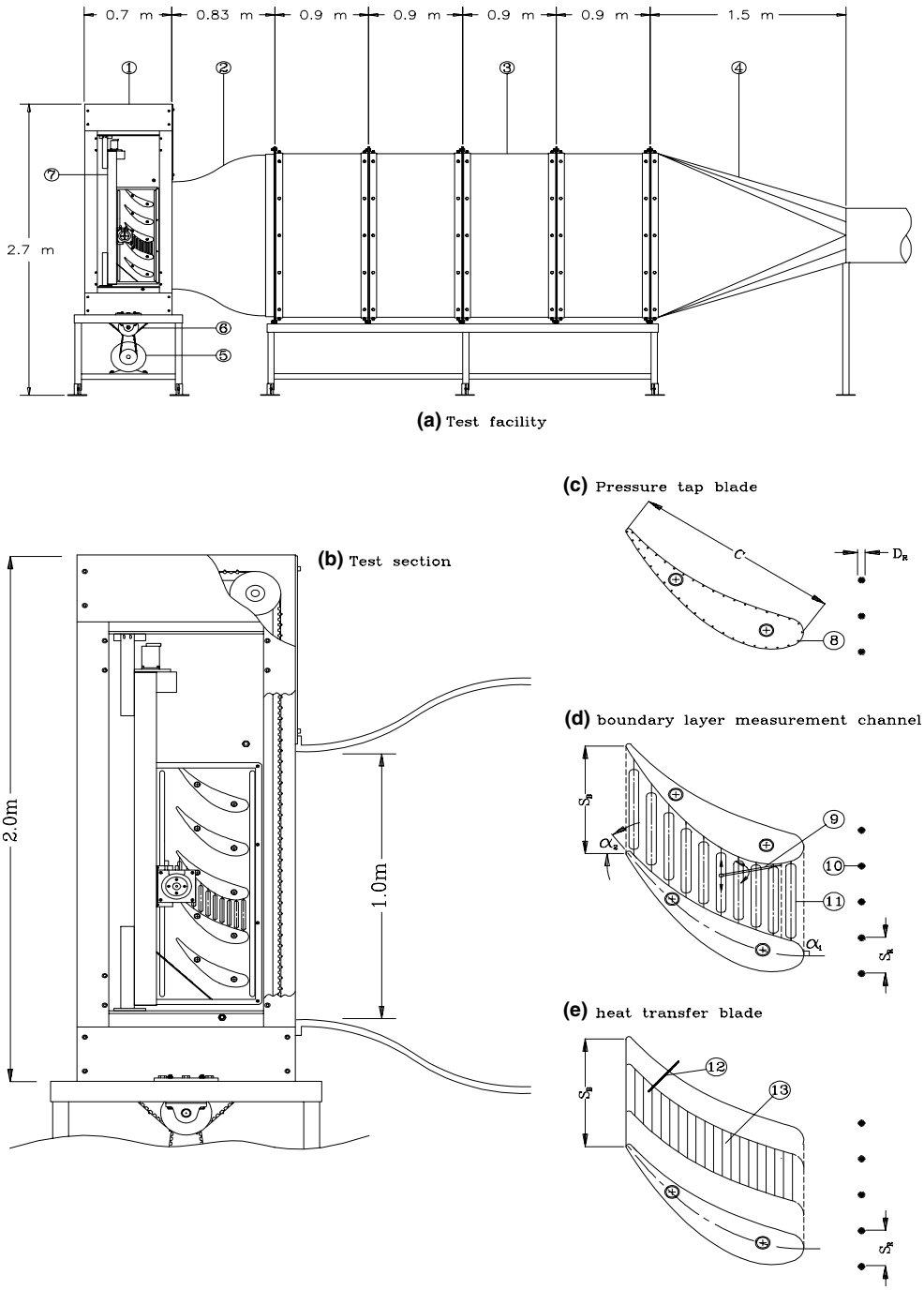

Fig. 1. Test facility: 1 – test section; 2 – nozzle; 3 – settling chamber; 4 – diffuser; 5 – motor; 6 – belt; 7 – traversing system; 8 – static pressure taps; 9 – boundary layer probe; 10 – wake generating rods; 11 – slots for longitudinal traverse of the probe; 12 – surface thermocouple; 13 – liquid crystal sheet.

2.2. Surface pressure distribution

The pressure distribution shown in Fig. 2 was taken by a multi-channel scannivalve for both the steady ($\Omega = 0.0$) and unsteady ($\Omega = 0.755$) case. The pressure distribution shows excellent repeatability under these two conditions. The pressure signals inherently signify the time-averaged pressure because of the internal

Table 1
Specifications of inlet flow and wake generator characteristics

Parameters	Values	Parameters	Values
Inlet velocity	$U_{in} = 15$ m/s	Blade exit metal angle	$\alpha_1 = 61.8°$
Blade inlet flow angle	$\alpha_1 = 0°$	Blade spacing	$S_B = 159.31$ mm
Blade height	$L = 200.0$ mm	Blade *Re*-number	$Re_c = 264,187$
Blade chord	$c = 281.8$ mm	Cascade flow coefficient	$\phi = 2.14$
Cascade solidity	$\sigma = 1.76$	Rod diameter	$D_R = 5.0$ mm
Steady reference point (no rods)	$s_R = \infty$ mm	Ω-parameter steady case	$\Omega = 0.0$
Cluster 1 rod spacing	$s_R = 160.0$ mm	Ω-parameter for cluster 1	$\Omega = 0.755$
Cluster 2 rod spacing	$s_R = 80.0$ mm	Ω-parameter for cluster 2	$\Omega = 1.51$
No. of rods in cluster 1	$n_R = 14$	No. of rods in cluster 2	$n_R = 21$

pneumatic damping effect of the connecting pipes to the transducer. The time-averaged pressure coefficient along the pressure and suction surfaces is plotted in this figure. On the suction surface (lower portion of the plot) the flow first accelerates sharply, reaches a minimum pressure coefficient at $s/s_0 \approx 0.25$, and then continuously decelerates at a moderate rate until the trailing edge is reached. On the pressure surface, the flow accelerates, reaches a local minimum pressure coefficient at $s/s_0 \approx 0.1$, and is subjected to deceleration until $s/s_0 \approx 0.25$ is reached. Beyond this point, the pressure gradient on the pressure surface remains at the accelerating situation, while decelerating pressure gradient prevails on the suction surface. This pressure gradient situation has a very significant effect on the boundary layer development, as seen later in the corresponding section of this paper.

2.3. Heat transfer experiments

A specially manufactured blade with an internal heater core is used for heat transfer experiments. A liquid crystal sheet is glued on the center portion of the blade for temperature measurements (see Fig. 1(e)). The power required for heating the heat transfer blade is supplied by a Sytron 10 V–200 A (maximum) dc power supply. The current passing through the test blade is measured with a multimeter connected across a shunt resistor. Two separate multimeters are used to measure the voltages in the circuit. One multimeter is connected across the output leads of the power supply to measure the voltage output, and the other is connected across the blade terminals. These two measurements are used to calculate the power losses in the cable resistance. The yellow band of the liquid crystal is used to record the data. The location of the yellow band is controlled through the power supply to the blade, and the voltage and the current readings across the blade terminals are recorded for different locations of the yellow band on the turbine blade.

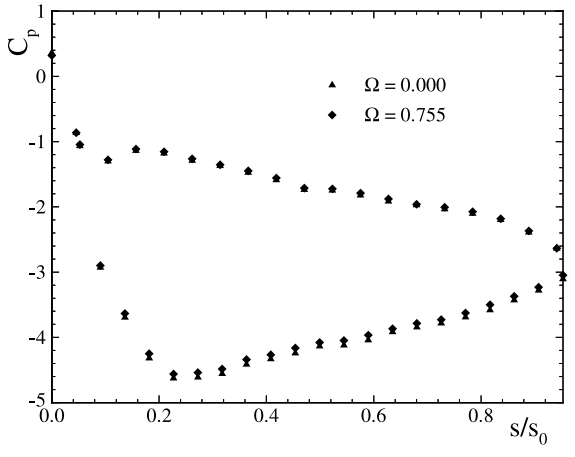

Fig. 2. Static pressure distributon at $Re_c = 264187$ under steady ($\Omega = 0.00$) and unsteady ($\Omega = 0.755$) flow conditions.

Apart from the *steady or no-rod* case, three different rod spacings are used for heat transfer experiments. They are 160, 80 and 40 mm, which corresponds to Ω values of 0.755, 1.51 and 3.02, respectively, at a belt speed of 6 m/s. The entire blade length is filled with rods of uniform spacing and data are collected separately for different wake passing frequencies. Time-averaged inlet turbulence intensities are measured for the above four frequencies. They are 1.0%, 3.16%, 5.234% and 9.93%, respectively. As mentioned at the beginning of this section, aerodynamic (boundary layer) data are taken *simultaneously* for Ω values of 0, 0.755 and 1.51. The data are collected for both the pressure and suction sides of the turbine blade.

3. Intermittency analysis

The intermittency distribution, which identifies whether the flow is laminar or turbulent inside the boundary layer, is calculated following the method of Hedley and Keffer [11]. Instantaneous velocities are used to identify this intermittency distribution. The instantaneous velocity is sensitized to increase its discriminatory capabilities between turbulent and non-turbulent parts of the signal. For this purpose, the second derivative of the velocity signal is used and squared for

further analysis. This is called the detector function, $S(t)$. Several other detector functions were used by Kowasznay et al. [12] and Antonia and Bradshaw [13]. A threshold level C is then applied to this detector function to distinguish between true turbulence and the signal *noise*.

$$I(t) = \begin{cases} 1, & \text{when } S(t) \geqslant C, \\ 0, & \text{when } S(t) < C. \end{cases} \tag{1}$$

After applying the threshold level to the detector function $S(t)$, the result is a random square wave with 0s representing the laminar case and 1s representing the turbulent behavior of the boundary layer. A threshold level, C, of 1.2 is used for all the data on the suction surface and a value of 0.5 is used on the pressure surface. In the absence of length scales, these two values are chosen from visual observations. Several other values of C are tested and little qualitative difference is seen in the intermittency distribution during transition. Though the intermittency values vary with different values of C, the important parameters like start and end of transition are not effected by C. The resulting square wave after applying the threshold is ensemble-averaged to get the ensemble-averaged intermittency as follows:

$$\langle \gamma_i(t_i) \rangle = \frac{1}{n} \sum_{j=1}^{n} I_{ij}(t_i), \tag{2}$$

where n is the number of revolutions of the wake generator for which the data are collected. For time-averaged intermittency, $\langle \gamma_i(t_i) \rangle$ is integrated with respect to time to arrive at

$$\overline{\gamma} = \frac{1}{T} \int_{t=0}^{T} \langle \gamma_i(t_i) \rangle \, \mathrm{d}t. \tag{3}$$

Fig. 3 shows the processing of instantaneous velocities. The ensemble-averaged intermittency distribution as a function of non-dimensional time is shown in the time-space diagrams shown in Figs. 4(a) and (b) for pressure surface and in Figs. 5(a) and (b) for suction surface for Ω value of 0.755 (160 mm spacing). Similar plots are seen for other rod spacing cases. Only the first three wakes are plotted for a better comparison of the effects of impinging wake frequency on the transition process. In these figures, the wakes with the highly vortical cores display intermittency values close to one indicating the turbulent character of the boundary layer at the particular instant of time that the wake impinges on the surface. Intermittency is approximately equal to zero outside the wake region near the leading edge showing the non-turbulent behavior of the flow. The wakes represented by thin strips pass through the turbine blade channel and periodically switch the boundary layer from laminar to turbulent and vice versa depending on the presence of the wakes. The periodic switching process

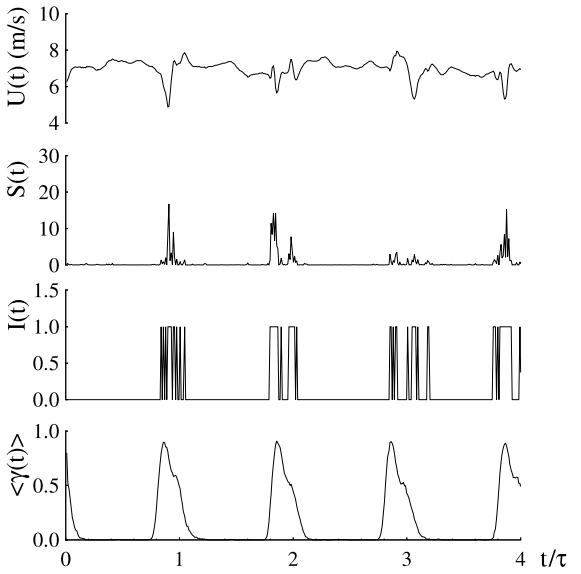

Fig. 3. Calculation of ensemble-averaged intermittency function from instantaneous velocities for $\Omega = 1.725$ at $y = 0.1$ mm.

takes place within the transition zone. In case of a lower reduced frequency $\Omega = 0.755$, shown in Fig. 4(a) (pressure surface), the transition onset starts at $s/s_0 = 0.0$ and extends to $s/s_0 \approx 0.9$. The natural transition of the boundary layer is affected by periodic passing of wakes and their frequency resulting in wake induced transition. The intermittency distributions in Figs. 4 and 5 clearly show the unsteady nature of the boundary layer transition. In this form, however, they cannot quantitatively describe the complex unsteady transition process. To establish the basic relations essential for a quantitative description of the unsteady boundary layer transition, we resort to the fundamental studies by Schobeiri and co-workers [19,22,23] that deal with the physics of steady and unsteady wake development in a curved environment. These studies clearly show that the turbulence structure of the steady and unsteady wake flow is determined by the wake defect, which is a Gaussian function. Following the above studies, we define a dimensionless parameter

$$\zeta = \frac{tU_{\mathrm{w}}}{b} = \frac{tS_{\mathrm{R}}}{\tau b} = \frac{\xi_2}{b} \text{ with } b = \frac{1}{\sqrt{\pi}} \int_{-\infty}^{+\infty} \Gamma \, \mathrm{d}\xi_2 \tag{4}$$

that relates the passing time, t, of a wake impinging on the plate surface with the wake passing velocity in the lateral direction, U_{w}, and the intermittency width, b. The latter is directly related to the wake width introduced by Schobeiri and co-workers [23]. In an analogous way to find the defect function, we define the relative intermittency, Γ, as

$$\Gamma = \frac{\langle \gamma_i(t_i) \rangle - \langle \gamma_i(t_i) \rangle_{\min}}{\langle \gamma_i(t_i) \rangle_{\max} - \langle \gamma_i(t_i) \rangle_{\min}}. \tag{5}$$

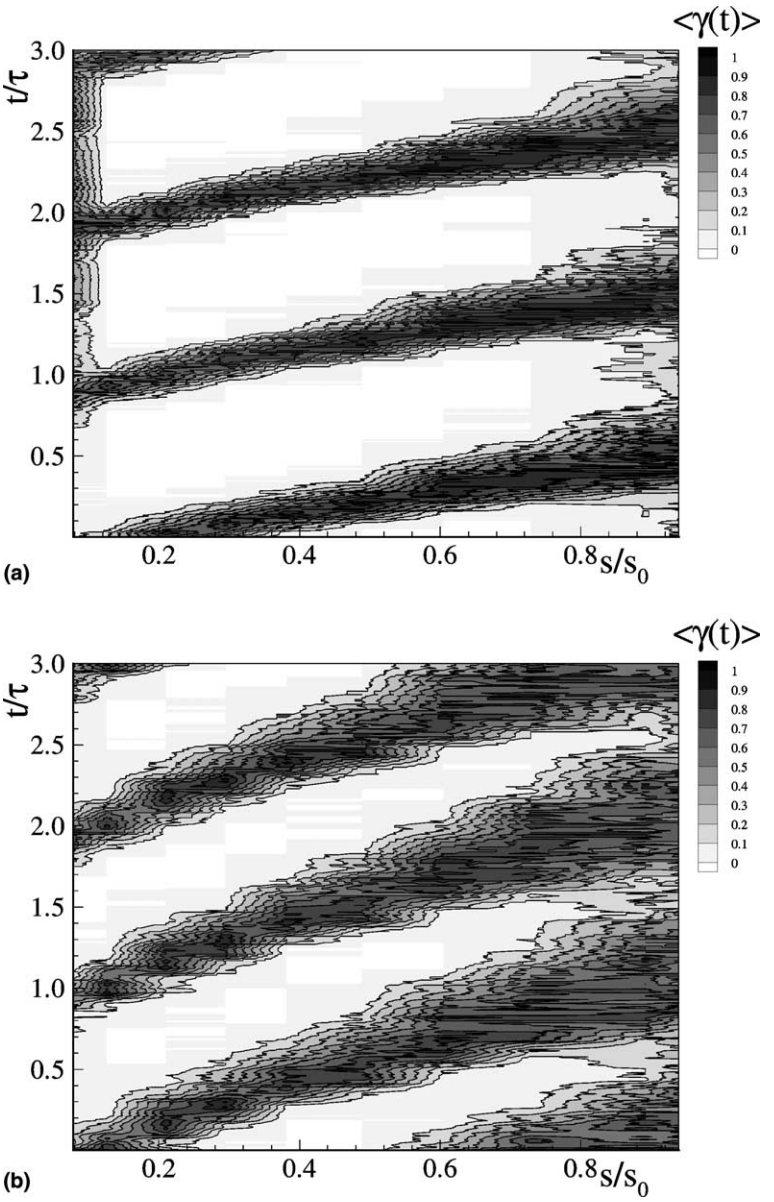

Fig. 4. Ensemble-averaged intermittency factor as a funtion of non-dimensional distance s/s_0 at $y = 0.1$ mm for (a) $\Omega = 0.755$ on the pressure surface of the turbine blade and (b) $\Omega = 1.51$ on the pressure surface of the turbine blade.

In the above equation, $\langle \gamma_i(t_i) \rangle$ is the time-dependent ensemble-averaged intermittency function, which determines the transitional nature of an unsteady boundary layer. The maximum intermittency $\langle \gamma_i(t_i)_{\max} \rangle$ exhibits the time-dependent ensemble-averaged intermittency value inside the wake vortical core. Finally, the minimum intermittency $\langle \gamma_i(t_i)_{\min} \rangle$ represents the ensemble-averaged intermittency values outside the wake vortical core. The relative intermittency function, Γ, is shown in Figs. 6(a) and (b), and 7(a) and (b), for frequency values of $\Omega = 0.755$ and $\Omega = 1.51$ on the pressure and suction surfaces, respectively, at a lateral distance from the blade surface of $y = 0.1$ mm, with the dimensionless longitudinal distance s/s_0 as a parameter. Similar results are observed for the other rod frequencies listed in Table 1. The symbols represent the experimental data. For the reduced frequencies and longitudinal positions presented in these plots, the measured relative intermittency functions for wakes impinging on plate surface follow very closely a Gaussian distribution, given by

$$\Gamma = e^{-\zeta^2}. \tag{6}$$

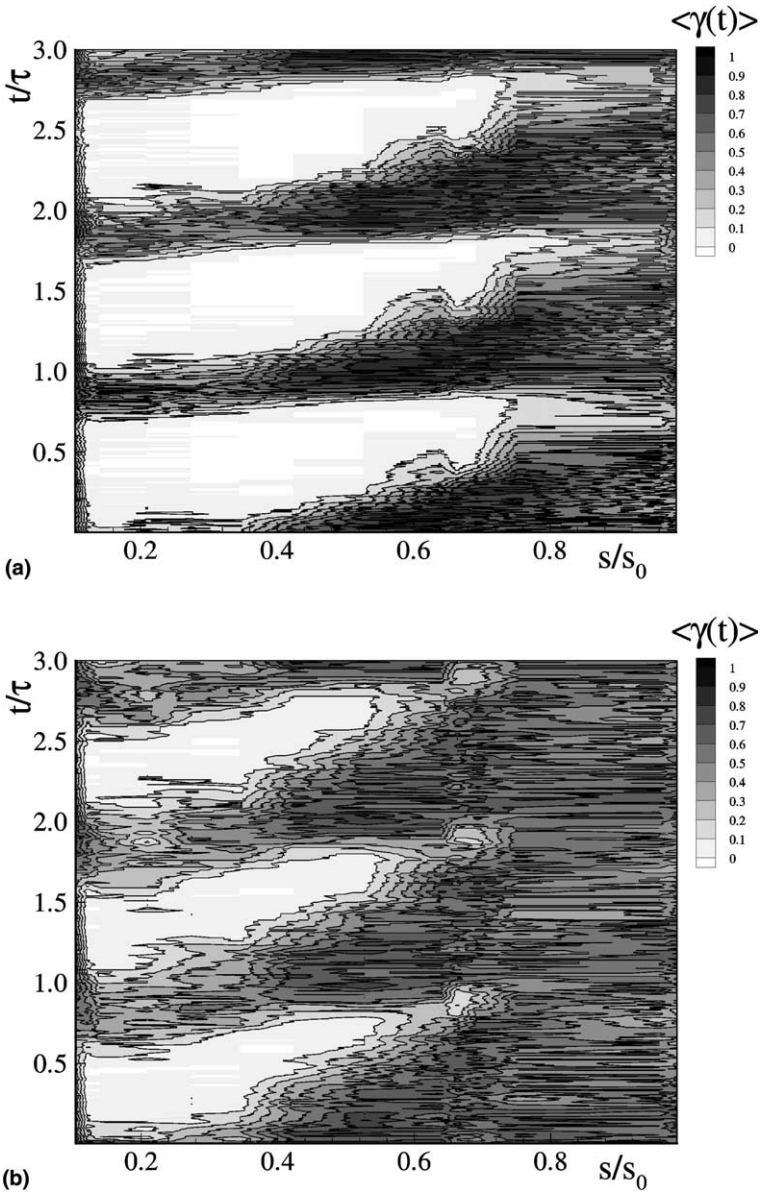

Fig. 5. Ensemble-average intermittency distribution as a funtion of s/s_0 at $y = 0.1$ mm for (a) $\Omega = 0.755$ on the suction surface of the turbine blade and (b) $\Omega = 1.51$ on the suction surface of the turbine blade.

Here, ζ is the non-dimensionalized lateral length scale. Using this function as a generally valid intermittency relationship for unsteady wake flows, the intermittency function $\langle \gamma_i(t_i) \rangle$ is completely determined if additional information about the minimum and the maximum intermittency functions $\langle \gamma_i(t_i) \rangle_{\min}$ and $\langle \gamma_i(t_i)_{\max} \rangle$ are available. The distribution of $\langle \gamma_i(t_i)_{\max} \rangle$ and $\langle \gamma_i(t_i)_{\min} \rangle$ in the streamwise direction are plotted in Figs. 8(a) and (b) for Ω values of 0.755 and 1.51 on the suction surface. For each particular streamwise location on the blade surface with a streamwise Reynolds number, for example $Re_{x,s} = 1 \times 10^5$, two corresponding distinctively different intermittency states are periodically present. At this location, $\langle \gamma_i(t_i)_{\max} \rangle$ corresponds to the condition when the wake with its high turbulence intensity core impinges on the plate surface. Once the wake has passed over the surface, the same streamwise location is exposed to a low turbulence intensity flow regime with an intermittency state of $\langle \gamma_i(t_i)_{\min} \rangle$, where no wake is present. As seen, $\langle \gamma_i(t_i)_{\min} \rangle$ tends to follow the course of steady (no-wake) intermittency distribution of Narasimha, with a gradual increase from an initial *non-turbulent* state with a value of

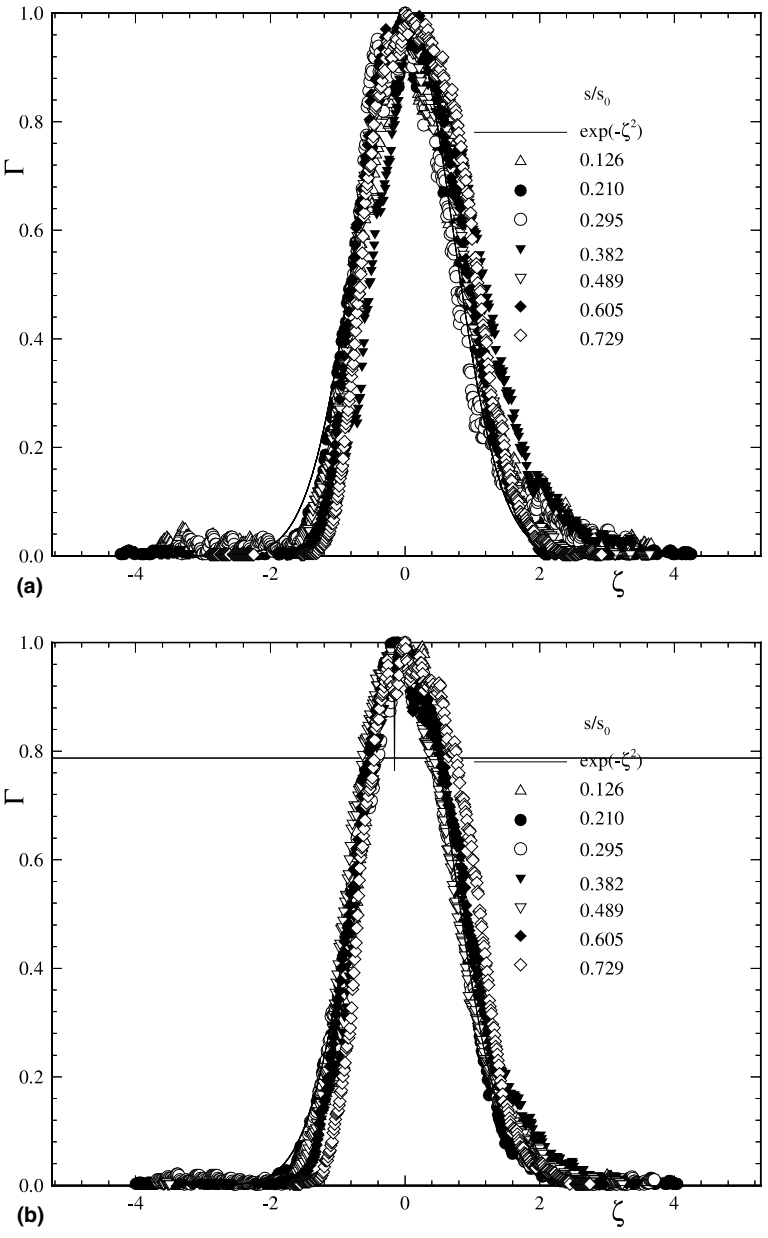

Fig. 6. Relative intermittency as a funtion of non-dimensionalized lateral coordinate for (a) $\Omega = 0.755$ at $y = 0.1$ on the pressure surface and (b) $\Omega = 1.51$ at $y = 0.1$ on the pressure surface.

zero approaching a final state of 0.5 in Fig. 8(b). The final state does not approach the fully turbulent value of 1.0 due to the *calming* effect of the boundary layer. For a lower wake frequency, Ω of 0.755 shown in Fig. 8(a), the minimum frequency raises to a value of 0.2 only. This is due to the boundary layer transition developing near the end of the blade. This is also seen in the contour plots in Fig. 4. There is hardly any interaction between the wakes for major portions of the blade, and the transition starts at s/s_0 value of about 0.8. This tendency is expected as $\langle \gamma_i(t_i)_{\min} \rangle$ is calculated outside the wake region where turbulence intensity is relatively small. On the other hand, $\langle \gamma_i(t_i)_{\max} \rangle$ reveals a fundamentally different behavior that needs to be discussed further. As Fig. 8(a) shows, the wake flow with an intermittency close to 1.0 impinges on the blade surface. By convecting downstream, its turbulent fluctuations undergo a strong damping by the wall shear stress forces. The process of damping continues until $\langle \gamma_i(t_i)_{\max} \rangle$ reaches a minimum. At this point, the wall shear forces are not able to further

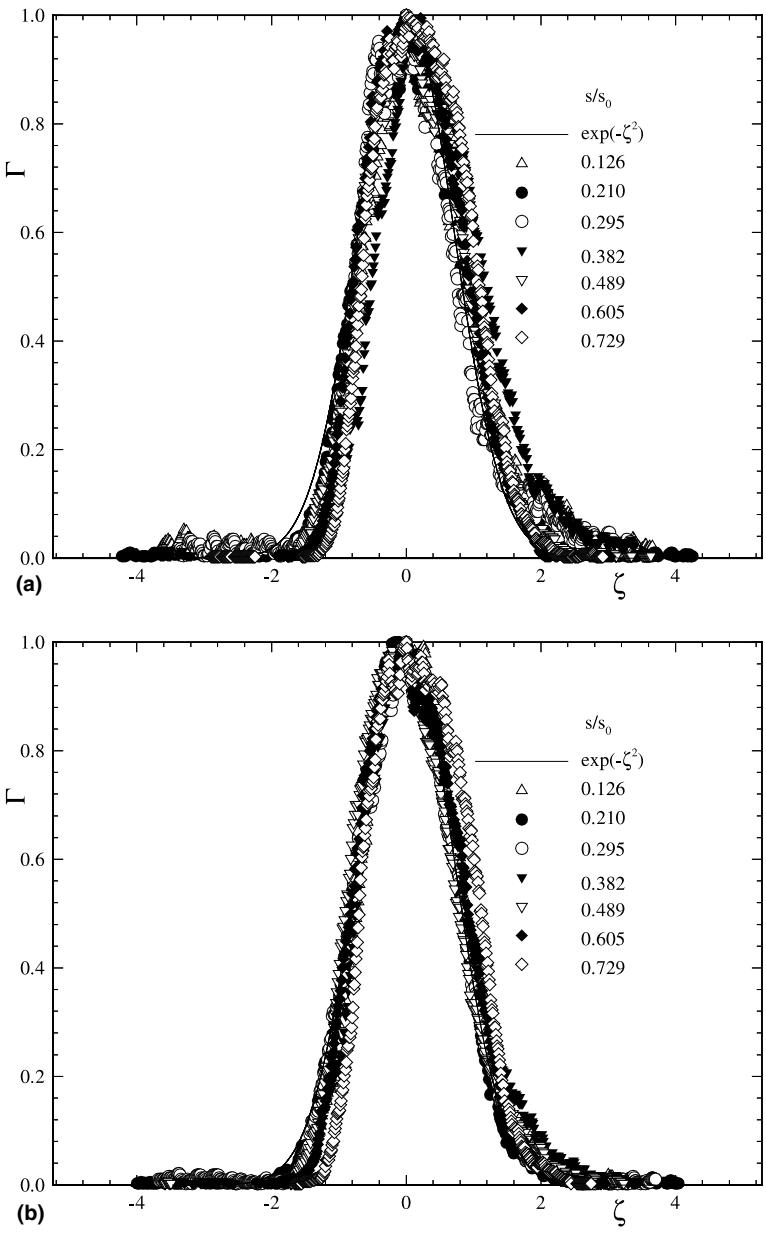

Fig. 7. Relative intermittency as a function of non-dimensionalized lateral coordinate for (a) $\Omega = 0.755$ at $y = 0.1$ on the suction surface and (b) $\Omega = 1.51$ at $y = 0.1$ on the suction surface.

suppress the turbulent fluctuations. As a consequence, the intermittency again increases to approach unity, showing the combined effect of *wake induced* and *natural transition* due to increased turbulence intensity level. It is apparent from Figs. 8(a) and (b) that there is an increase in the value of minimum intermittency $\langle \gamma_i(t_i)_{\min} \rangle$ as the wake passing frequency is increased. Also, the viscous wall effect/damping has a more pronounced effect on $\langle \gamma_i(t_i)_{\max} \rangle$ for a higher wake passing frequency. The overall effect is an increase in the average intermittency value, which is shown in Figs. 8(a) and (b). The maximum intermittency is described by

$$\langle \gamma(t) \rangle_{\max} = 1.0 - c_1 \mathrm{e}^{-\left(\frac{Re_x - Re_{x,s}}{Re_{x,s} - Re_{x,e}}\right)^2}, \tag{7}$$

where c_1 is dependent on Ω and represents the extent of the wall damping effect on $\langle \gamma_i(t_i)_{\max} \rangle$. The minimum intermittency described by

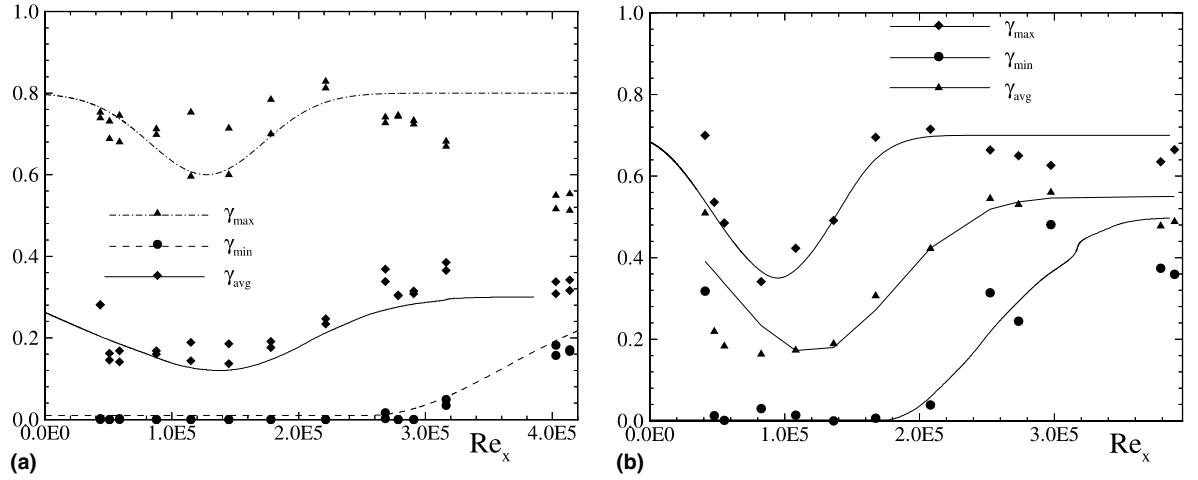

Fig. 8. (a) Maximum, minimum, and time-averaged intermittency as a function of longitudinal Reynolds number for $\Omega = 0.755$ at $y = 0.1$ mm on the suction surface of the turbine blade. (b) Maximum, minimum, and time-averaged intermittency as a function of longitudinal Reynolds number 0 for $\Omega = 1.51$ at $y = 0.1$ mm on the suction surface of the turbine blade.

$$\langle \gamma(t) \rangle_{\min} = c_2 \left[1.0 - \mathrm{e}^{-\left(\frac{Re_x - Re_{x,s}}{Re_{x,s} - Re_{x,e}} \right)^2} \right], \tag{8}$$

where c_2 is again dependent on Ω and is introduced as the asymptotic value of the minimum intermittency. The time-averaged intermittency is described by

$$\overline{\gamma} = c_4 \left[1.0 - c_3 \mathrm{e}^{-\left(\frac{Re - Re_{x,s}}{Re_{x,s} - Re_{x,e}} \right)^2} \right]. \tag{9}$$

Constants c_3 and c_4 give the combined effect of c_1 and c_2 for the time-averaged intermittency $\overline{\gamma}$. These constants are not universal constants and differ for different wake passing frequencies. Also, the Reynolds numbers at the start and end of transition, $Re_{x,s}$ and $Re_{x,e}$, differ for different wake frequencies.

4. Implementation of the transition model into calculation procedures

The developed transition model can be implemented into any Navier–Stokes or differential boundary layer code. We have chosen TEXSTAN, which simultaneously solves differential equations of continuity, momentum, and energy. All these equations are time-averaged and written to describe the flow over an axisymmetric body. The time-averaged continuity equation is given by

$$\frac{\partial}{\partial x}(r\rho U) + \frac{\partial}{\partial y}(r\rho V) = 0. \tag{10}$$

The time-averaged momentum equation in the x-direction is

$$\rho U \frac{\partial U}{\partial x} + \rho V \frac{\partial U}{\partial y} = -\frac{\mathrm{d}p}{\mathrm{d}x} + \frac{1}{r}\frac{\partial}{\partial y}\left[r\left(\mu \frac{\partial U}{\partial y} - \rho \overline{u'v'} \right) \right]. \tag{11}$$

In this momentum equation, the turbulent shear stress is modeled by the eddy diffusivity for momentum and is defined

$$-\overline{u'v'} = \epsilon_{\mathrm{M}} \frac{\partial U}{\partial y} = \frac{\mu_{\mathrm{t}}}{\rho} \frac{\partial U}{\partial y}, \tag{12}$$

where μ_{t} is the turbulent viscosity, which combines with the laminar viscosity to give

$$\mu_{\mathrm{eff}} = (\mu + \mu_{\mathrm{t}}) = \rho(\nu + \epsilon_{\mathrm{M}}). \tag{13}$$

Similarly, after introducing the concept of eddy diffusivity for heat, ϵ_{H}, the energy equation becomes

$$\rho U \frac{\partial I^*}{\partial x} + \rho V \frac{\partial I^*}{\partial y} = \frac{1}{r}\frac{\partial}{\partial y}\left\{ r\left[\frac{\mu_{\mathrm{eff}}}{Pr_{\mathrm{eff}}} \frac{\partial I^*}{\partial y} + \frac{\mu_{\mathrm{eff}}}{J}\left(1 - \frac{1}{Pr_{\mathrm{eff}}} \right) \frac{\partial}{\partial y}\left(\frac{U^2}{2} \right) \right] \right\}, \tag{14}$$

where I^* is the stagnation enthalpy and Pr_{eff} is the effective Prandtl number defined as

$$Pr_{\mathrm{eff}} = \frac{\mu_{\mathrm{eff}}}{(k/c)_{\mathrm{eff}}} = \frac{1 + (\epsilon_{\mathrm{M}}/\nu)}{(1/Pr) + (\epsilon_{\mathrm{M}}/\nu)(1/Pr_{\mathrm{t}})} \tag{15}$$

and Pr_{t} is the turbulent Prandtl number given by

$$Pr_{\mathrm{t}} = \frac{\epsilon_{\mathrm{M}}}{\epsilon_{\mathrm{H}}} \tag{16}$$

with ϵ_{M} and ϵ_{H} as the eddy diffusivities for momentum and heat transfer. The eddy viscosity term is modeled

through the mixing length theory and the above intermittency model is implemented by

$$\epsilon_M = \gamma l^2 \left| \frac{\partial U}{\partial y} \right|, \tag{17}$$

where l is the mixing length and γ is the intermittency. The solution process uses Patankar–Spalding's [24] omega (non-dimensional stream function) transformation. In stream function coordinates, the momentum equation without the body forces becomes

$$U\frac{\partial U}{\partial x} + U\frac{\partial}{\partial \psi}\left[U v_{\text{eff}} \frac{\partial U}{\partial \psi}\right] = -\frac{1}{\rho}\frac{\mathrm{d}p}{\mathrm{d}x}. \tag{18}$$

The boundary layer equations are integrated after non-dimensionalizing the stream function and solved numerically.

5. Results and discussions, aerodynamic study

5.1. Experimental results, velocity distribution

Fig. 9 is a representative diagram of ensemble-averaged velocity profiles inside the boundary layer on the suction surface of the turbine blade at a constant streamwise location and different y-locations. For the clarity, only the first five wakes are shown in the figure. Outside the boundary layer ($y = 10$ mm), wakes are characterized by relatively high random fluctuations compared to the flow regime outside the wake. Velocity outside the wakes is free of disturbances, which is typical of laminar flow in the free-stream. The random fluctuations inside the wake vortical core are amplified inside the boundary layer close to the wall. A closer look at the wake propagation is shown in Figs. 10(a) and (b) for two different wake passing frequencies of $\Omega = 0.755$ and 1.51 at a lateral distance of $y = 2.5$ mm above the plate surface. The velocity is normalized with respect to the velocity of corresponding steady case ($\Omega = 0$) at $y = 2.5$ mm. For the first half of the profile length on the pressure surface, $s/s_0 = 0.295$ and 0.489, the velocity distributions in Fig. 10(a) exhibit an asymmetric behavior reflecting the effect of a strong curvature on the velocity distribution. The wake development and decay as it convects downstream is also seen in this figure. The process of wake development and decay observed in this investigation is very similar to the one investigated theoretically and experimentally by Schobeiri et al. [23].

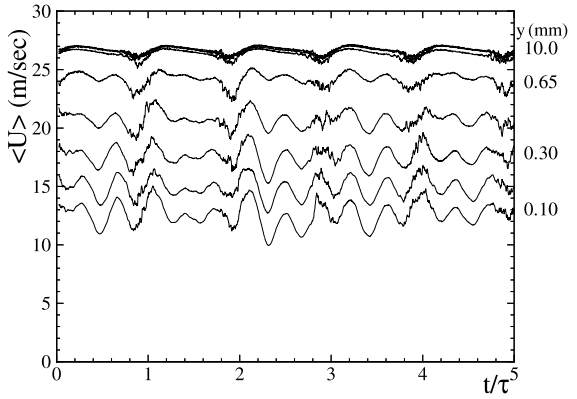

Fig. 9. Ensemble-average velocity distribution as a function of non-dimensional time at different y-locations at $s/s_0 = 0.274$ for $\Omega = 0.755$.

5.2. Experimental results, intermittency distribution

The entire set of ensemble-averaged data was utilized to generate the temporal–spatial distribution of the ensemble-averaged turbulence intermittency. Figs. 4 and 5 show a few cases as representative examples at $y = 0.1$ mm for Ω values of 0.755 and 1.51, respectively. As shown in Fig. 4, for the pressure surface ($\Omega = 0.755$, 160 mm spacing), the boundary layer is periodically disturbed by the wakes that periodically produce high turbulence strips and *extended becalmed regions*. These extended becalmed regions were produced by strong damping of turbulence fluctuations in the wall region that lead to an exponential decrease of the maximum intermittency $\langle \gamma_i(t_i) \rangle_{\max}$. As seen in Fig. 4(a), the wake strips with their characteristic vortical cores are separated from the non-vortical regions outside the wakes indicating the absence of any visible interaction of wakes throughout the pressure surface of the turbine blade for the reduced frequency of $\Omega = 0.755$ (160 mm spacing). Increasing the frequency Ω of the wake by reducing the rod spacing (Fig. 5(b) with $\Omega = 1.51$, 80 mm spacing) results in an earlier transition start compared to the above 160 mm rod spacing. In the case of the suction surface shown in Fig. 5(a) for $\Omega = 0.755$, the transition seems to start at about s/s_0 value of 0.75. Similar to the pressure surface cases, increasing the frequency Ω of the wake by reducing the rod spacing (Fig. 5(b) with $\Omega = 1.51$, 80 mm spacing) results in an earlier transition start compared to the above 160 mm rod spacing. Two mechanisms are considered instrumental in affecting the above transition start. The first one is an earlier mixing of the wakes due to the reduction of their spacing, which leads to higher free-stream turbulence and inherently affects the onset of the transition. The second mechanism is the increased impinging frequency of the primary wake strips that introduce an excessive turbulent kinetic energy transport to the boundary layer, causing a shift of transition start towards the leading edge. It is conceivable that the combination of these two mechanisms would contribute to the shift of the transition start. A further increase of Ω results in a higher free-stream turbulence and increased impinging frequency and, thus, a significant shift of the transition toward the

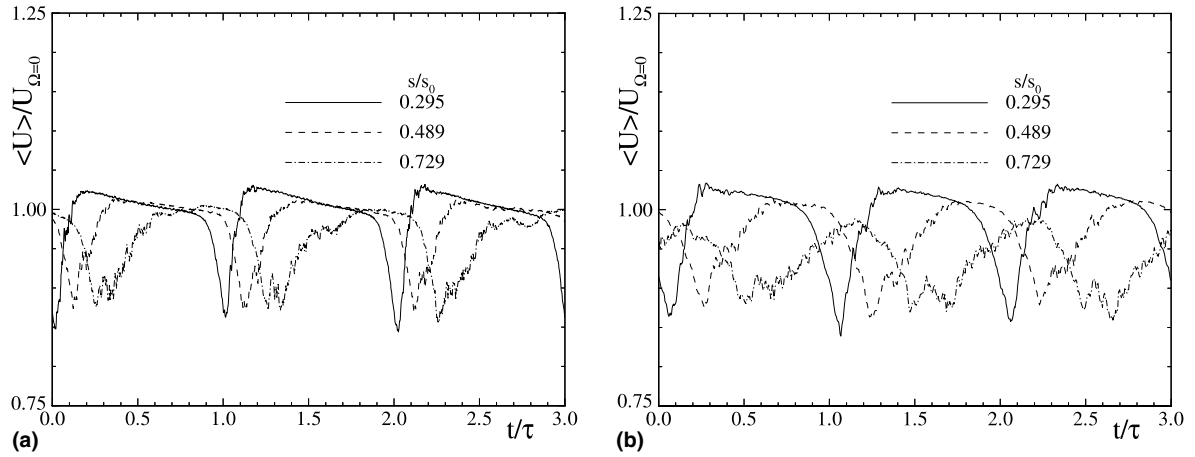

Fig. 10. Ensemble-average velocity on pressure surface at $y = 2.5$ mm for (a) $\Omega = 0.755$ and (b) $\Omega = 1.51$.

leading edge as the consequence of the mechanisms discussed above. A similar turbulence intermittency pattern is observed for other y-positions.

6. Results and discussions, heat transfer study

6.1. Heat transfer coefficient calculation

The heat transfer coefficient is calculated from the following expression:

$$h = \frac{Q_{\text{foil}} - Q_{\text{rad}}}{(T_{\text{yl}} - T_{\infty})}, \tag{19}$$

where Q_{rad} is the radiation heat loss from the surface of the turbine blade, Q_{foil} is the heat flux of the inconel foil, T_{yl} is the yellow line temperature and T_{∞} is the free-stream temperature. Q_{foil} and Q_{rad} are given by

$$Q_{\text{foil}} = \frac{VI}{A_{\text{foil}}} \tag{20}$$

and

$$Q_{\text{rad}} = \epsilon\sigma(T_{\text{yl}}^4 - T_{\infty}^4) \tag{21}$$

with V as the voltage across blade terminals, I as the current supplied from the power supply, ϵ as the emissivity, and σ as the Stefan–Boltzmann constant. A_{foil} is equal to the total heat transfer surface area of the blade surface. Finally, the Stanton number is defined by

$$St = \frac{h}{\rho C_{\text{p}} \overline{U}}. \tag{22}$$

6.2. Heat transfer coefficient distribution

As indicated previously, we used liquid crystal technique developed by Hippensteele et al. [25] for heat transfer measurement. This is being routinely applied by numerous researchers because it has the advantage of not affecting the turbulence structure at the surface, as thermocouples or surface mounted hot-wire/film probes do. However, its slow response does not allow extracting valuable unsteady information. As a result, only time-averaged response can be acquired in unsteady cases. Stanton number distributions on the suction and pressure surfaces of the turbine blade for four different wake passing frequencies of $\Omega = 0$, 0.755, 1.51, and 3.02 that correspond to the spacings of, 40, 80, 160 mm and ∞ are shown in Fig. 11. The uncertainties with the heat transfer coefficients are 6.8%. These results confirm the recent investigations on the effect of unsteady flows on heat transfer distribution of turbine blade by Han et al. [26]. The enhancement of the heat transfer coefficient with increase in the wake passing frequency is clearly apparent from these results. For the steady case on the suction surface, the transition starts near the trailing edge and the beginning of the transition point moves toward the leading edge as wake passing frequency is increased. There is also a consistent increase in the heat transfer coefficient with increase in wake passing frequency, but there is no apparent transition phenomena occurring on the pressure surface of the turbine blade, which is also evident from the aerodynamic measurements shown in Figs. 4(a) and (b).

The expressions from the intermittency analysis of the aerodynamic data are implemented in the boundary layer code, TEXSTAN, and the results are compared with the experimental data. Figs. 11(a) and (b) show the heat transfer distribution on the suction surface for Ω values of 0.755 and 1.51. Three lines that predict the heat transfer coefficient corresponding to the maximum, minimum, and average intermittency functions are plotted in these figures along with the experimental data shown by symbols. Again, the three lines that correspond to the maximum, minimum, and average inter-

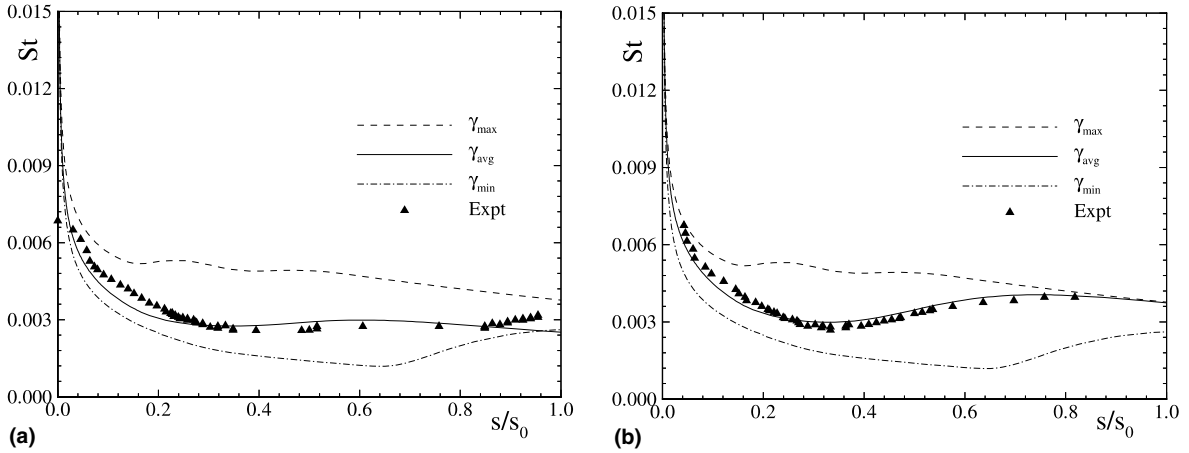

Fig. 11. Stanton number distribution on the suction surface of the turbine blade as a function of axial distance for (a) $\Omega = 0.755$ and (b) $\Omega = 1.51$.

mittency distributions are shown in these figures. The upper dashed curve represents the streamwise Stanton number distribution when the plate is subjected to an inlet flow intermittency state of $\langle \gamma(t) \rangle_{max}$. On the other hand, when the plate is subjected to $\langle \gamma(t) \rangle_{min}$, the lower point-dashed curve depicts its Stanton number distribution. However, because of the periodic character of the inlet flow associated with unsteady wakes, the plate would experience a periodic change of heat transfer represented by upper and lower Stanton number curves (dashed and point-dashed line) as an envelope. The liquid crystal responds to this periodic event with time-averaged signals. This time-averaged result is reflected by the solid line, which is given by corresponding time-averaged intermittency. As seen, a reasonably good agreement is found for the entire laminar and transitional portions on the suction side of the turbine blade.

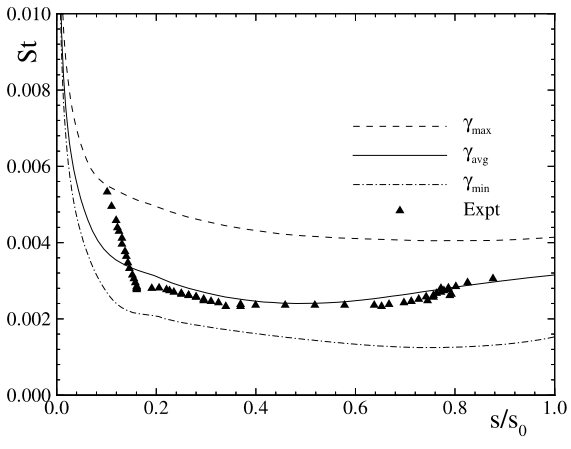

Fig. 12. Stanton number distributions on the pressure surface of the turbine blade as a function of axial distance for $\Omega = 0.75$.

Good agreement is seen between the average predicted heat transfer coefficient and the experimental data. Fig. 12 shows the heat transfer distribution on the pressure surface for Ω value of 0.755. Three lines that predict the heat transfer coefficient corresponding to the maximum, minimum, and average intermittency functions are plotted on this figure along with the experimental data that is shown in symbols. There is good agreement of the average predicted heat transfer coefficient with the experimental data, except in the leading edge region where the experimental values are higher than the predicted values.

7. Conclusions

A comprehensive investigation into the effect of periodic unsteady wakes on the boundary layer and heat transfer characteristics of a turbine blade is made for different wake passing frequencies. Both aerodynamic and heat transfer measurements were conducted that give an insight into wake induced boundary layer transition. The analysis of the boundary layer experimental data revealed the universal character of the relative intermittency function which is described by a Gausssian function. Based on the intermittency function, an unsteady transition model was developed and implemented into an existing boundary layer code, and the results were compared with the measurement. The following conclusions were drawn:

1. The periodic unsteady flow changed the boundary layer transition from natural transition to wake induced transition depending on the presence of a turbulent core inside the wake region.
2. The relative intermittency factor followed a Gaussian distribution. The minimum intermittency factor,

$\langle\gamma_{min}\rangle$, represented the boundary layer behavior between the turbulent wake strips. It was shown to follow the natural transition process as the free-stream was almost non-turbulent. On the other hand, $\langle\gamma_{max}\rangle$, being the value inside the turbulent core, started with a value of $\approx$1.0 and went through a minimum. This was due to the viscous damping of the turbulent core by the boundary layer.

3. The transition model implemented into a boundary layer code resulted in an accurate prediction of aerodynamics and heat transfer along the curved plate and the turbine blade.
4. Based on these results, the implementation of the model into a Navier–Stokes code is expected to deliver the results with high accuracy.

References

[1] H.W. Emmons, The laminar-turbulent transition in boundary layer – part I, J. Aero. Sci. 18 (1951) 490–498.

[2] S. Dhawan, R. Narasimha, Some properties of boundary layer flow during the transition from laminar to turbulent motion, J. Fluid Mech. 3 (1958) 418–436.

[3] B.J. Abu-Ghannam, R. Shaw, Natural transition of boundary layers – the effects of turbulence, pressure gradient and flow history, J. Mech. Eng. Sci. 22 (1980) 213–228.

[4] J.P. Gostelow, A.R. Blunden, Investigations of boundary layer transition in an adverse pressure gradient, ASME J. Turbomachinery 111 (1989) 366–375.

[5] K. Dullenkopf, R.E. Mayle, ASME Paper No. 94-GT-174, 1994.

[6] J.P. Gostelow, N. Melwani, G.J. Walker, Effects of streamwise pressure gradient on turbulent spot development, ASME Paper No. 95-GT-303, 1995.

[7] G.J. Walker, Modeling of transitional flow in laminar separation bubbles, in: 9th International Symposium Air Breathing Engines, 1989, pp. 539–548.

[8] H.P. Hodson, Modeling unsteady transition and its effects on profile loss, J. Turbomachinery 112 (1990) 691–701.

[9] D.E. Paxson, R.E. Mayle, Laminar boundary layer interaction with an unsteady passing wake, J. Turbomachinery 113 (1991) 419–427.

[10] U. Orth, Unsteady boundary-layer transition in flow periodically disturbed by wakes, ASME Paper No. 92-GT-283, 1992.

[11] B.T. Hedley, F.J. Keffer, Turbulent/non-turbulent decisions in an intermittent flow, J. Fluid Mech. 64 (1974) 625–644.

[12] L.S.G. Kovasznay, V. Kibens, R.F. Blackwelder, J. Fluid Mech. 41 (1970) 283.

[13] R.A. Antonia, P. Bradshaw, Imp. College Aero. Report No. 71-04, 1971.

[14] P. Bradshaw, J. Murlis, Imp. College Aero. Technical Note, No. 73-108, 1973.

[15] R.E. Mayle, The role of laminar–turbulent transition in gas turbine engines, J. Turbomachinery 113 (1991) 509–537.

[16] B.E. Launder, D.B. Spalding, Mathematical Models of Turbulence, Academic Press, New York, 1972.

[17] M.E. Crawford, W.M. Kays, STAN5 (TEXSTAN version) – A Program for Numerical Computation of Two Dimensional Internal and External Boundary Layer Flow, NASA CR-2742, 1976.

[18] R.C. Schmidt, S.V. Patankar, Simulating boundary layer transition with low-Reynolds number k–ϵ turbulence models: part I – an evaluation of prediction characteristics; part II – an approach to improving the predictions, J. Turbomachinery 113 (1991) 10–26.

[19] M.T. Schobeiri, K. Pappu, L. Wright, Experimental study of the unsteady boundary layer behavior on a turbine cascade, ASME Paper No. 95-GT-435, 1995.

[20] M.T. Schobeiri, E. McFarland, F. Yeh, Aerodynamic and heat transfer investigations on a high Reynolds number turbine cascade, NASA TM-103260, 1991.

[21] J. John, T. Schobeiri, A simple and accurate method of calibrating X-probes, ASME J. Fluids Eng. 115 (1993) 148–152.

[22] M.T. Schobeiri, K. Read, J. Lewalle, Effect of unsteady wake passing frequency on boundary layer transition: experimental investigation and wavelet analysis, ASME Paper No. 95-GT-437, 1995b.

[23] M.T. Schobeiri, J. John, K. Pappu, Development of two dimensional wakes within curved channel: theoretical framework and experimental investigations, ASME J. Turbomachinery 118 (1996) 506–518.

[24] S.V. Patankar, D.B. Spalding, Heat and Mass Transfer in Boundary Layers, second ed., International Textbook Company, London, 1970.

[25] S.A. Hippensteele, L.M. Russell, S. Stepka, Evaluation of a method for heat transfer measurements and thermal visualization using a composite of a heater element and liquid crystals, ASME J. Heat Transfer 105 (1981) 184–189.

[26] J.-C. Han, L. Zhang, S. Ou, Influence of unsteady wake on heat transfer coefficient from a gas turbine blade, ASME J. Heat Transfer 115 (1993) 904–911.